Supporting information

Crystal facet-dependent activity of *h*–WO_3 for selective conversion of furfuryl alcohol to ethyl levulinate

Guoming Gao[a], Mingxuan Lv[a], Yuewen Shao[a], Guanggang Gao[a], Hui Zhao[b], Shu Zhang[c], Yi Wang[d], Ran Duan[e], Qifeng Chen[a,*], Xun Hu[a,*]

[a] School of Material Science and Engineering, University of Jinan, Jinan, 250022, P. R. China.

[b] Institute of Surface Analysis and Chemical Biology, University of Jinan, Jinan, 250022, P. R. China.

[c] College of Materials Science and Engineering, Nanjing Forestry University, Nanjing 210037, Jiangsu, china.

[d] State Key Laboratory of Coal Combustion, Huazhong University of Science and Technology, Wuhan, 430074, P.R. China.

[e] Institute of Chemistry Chinese Academy of Sciences, Beijing, 100190, China.

*Corresponding author. qfchen@126.com (Q. Chen); Xun.Hu@outlook.com (X. Hu).

Number of Tables: 2

Number of Figures: 9

Number of Pages: 12

Table S1 Peak area distribution of hexagonal WO_3 with different crystal planes after infrared peak separation

Entry	Catalyst	Peak area		
		818 cm^{-1} (W=O)	678 cm^{-1} (O–W–O)	Total
1	WO_3-nanobelts	58.5	20.2	78.7
2	WO_3-nanosheets	14.7	99.0	113.7
3	WO_3-nanoparticles	92.3	25.2	117.5

Table S2 Deconvoluted peaks of O1s over different samples

Sample	Peak	Position (eV)	Area	FWHM (eV)	(%)
nanoparticle	–OH	531.8	11710.23	1.91	23.58
	W=O	530.3	44453.29	1.58	69.76
	O–W	528.8	7555.67	1.33	9.98
nanobelt	–OH	532	959.65	0.96	1.39
	W=O	530.2	30399.92	1.49	44.00
	O–W	528.83	37725.5	1.31	54.61
nanosheet	–OH	532.2	6006.34	2.59	6.72
	W=O	530.2	65849.6	1.81	73.68
	O–W	528.4	17515.06	1.73	19.60

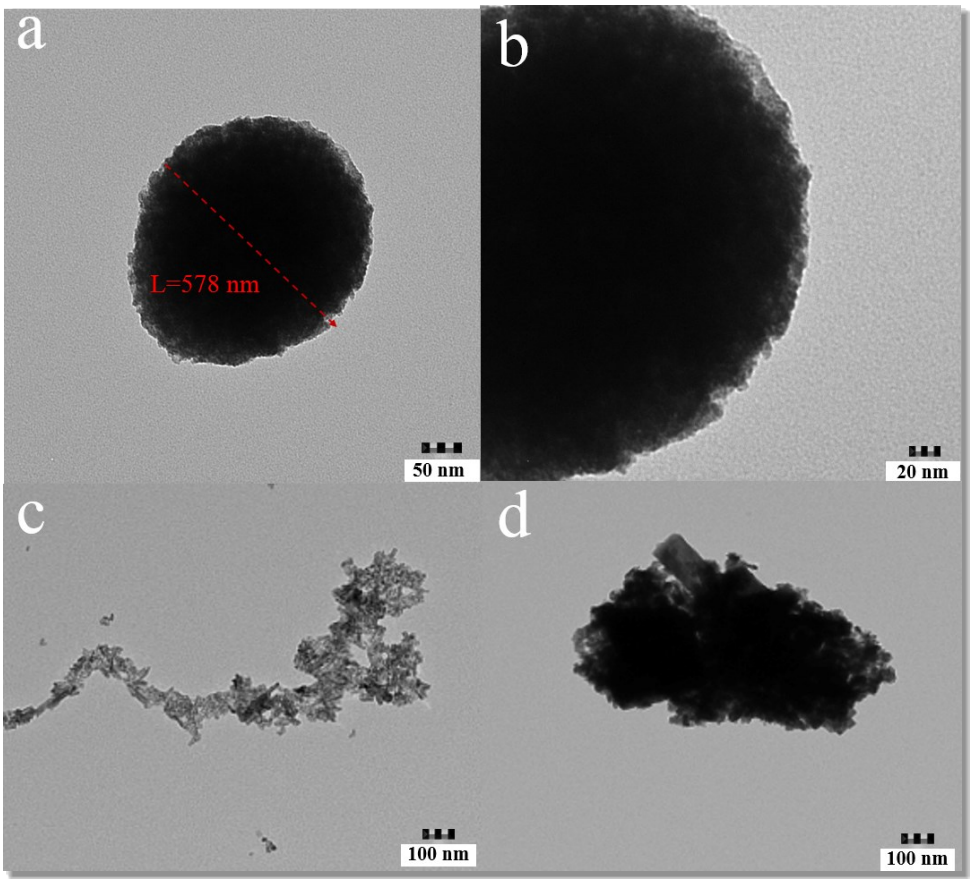

Figure S1 a and b: TEM of WO_3 Nanoparticles (after four circles); **c**: TEM of WO_3 nanobelts (after one circle); **d**: TEM of WO_3 Nanosheets (after one circle).

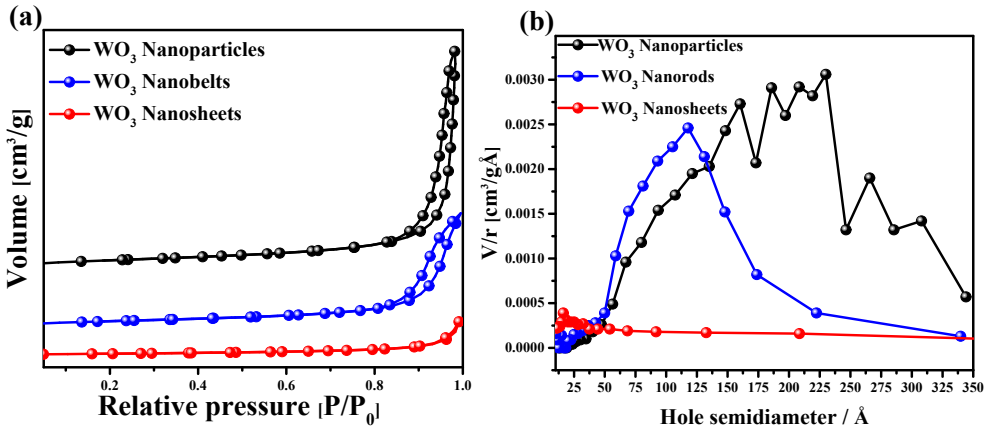

Figure S2 The isothermal curves and pore size distribution diagram of BJH desorption hole over the WO_3 catalysts with different morphologies. (a) The isothermal curves. (b) pore size distribution diagram of BJH desorption hole.

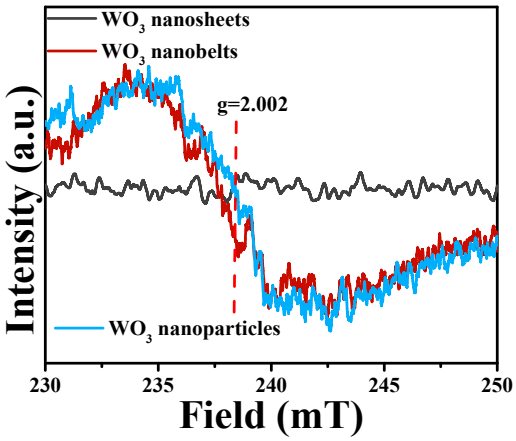

Figure S3 EPR spectra of hexagonal WO_3 with different crystal facets exposed.

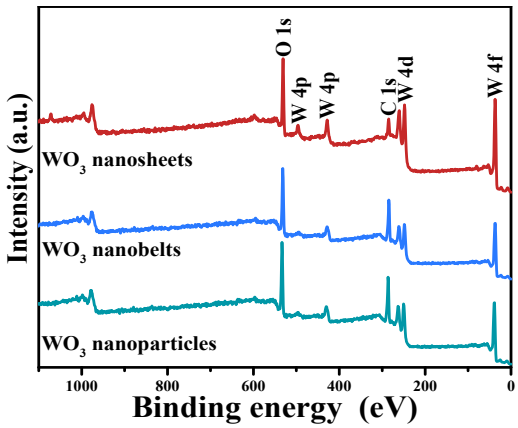

Figure S4 High resolution XPS survey spectra over the *h*-WO_3 catalysts with different morphologies.

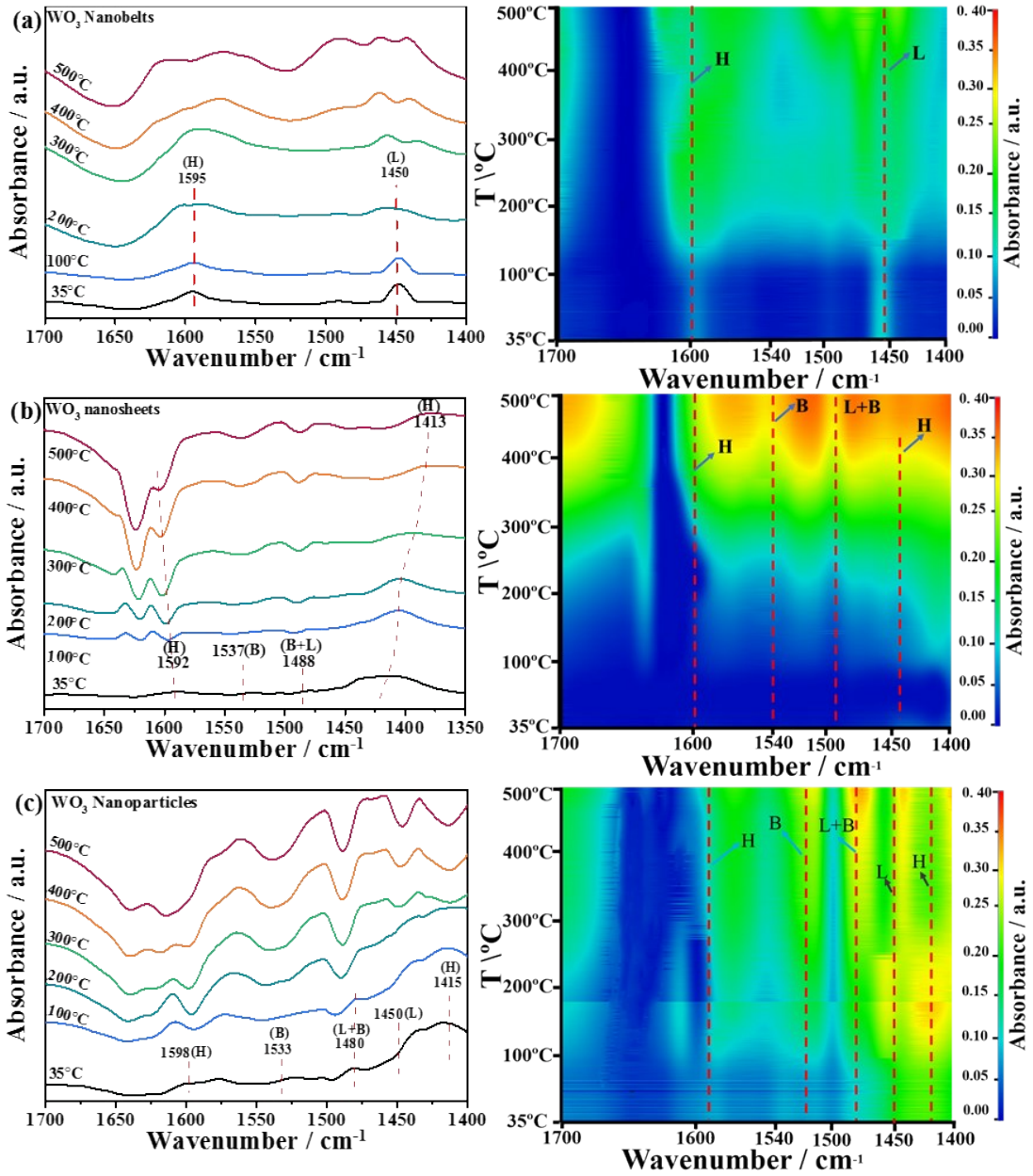

Fig. S5 In–situ DRIFTS of pyridine desorption of *h*-WO_3 catalysts with different morphologies, (a) *h*-WO_3 nanobelts, (b) *h*-WO_3 nanosheets, and (c) *h*-WO_3 nanoparticles. B: Brønsted acid sites; L: Lewis acid sites; H: Hydrogen-bonded pyridine molecules.

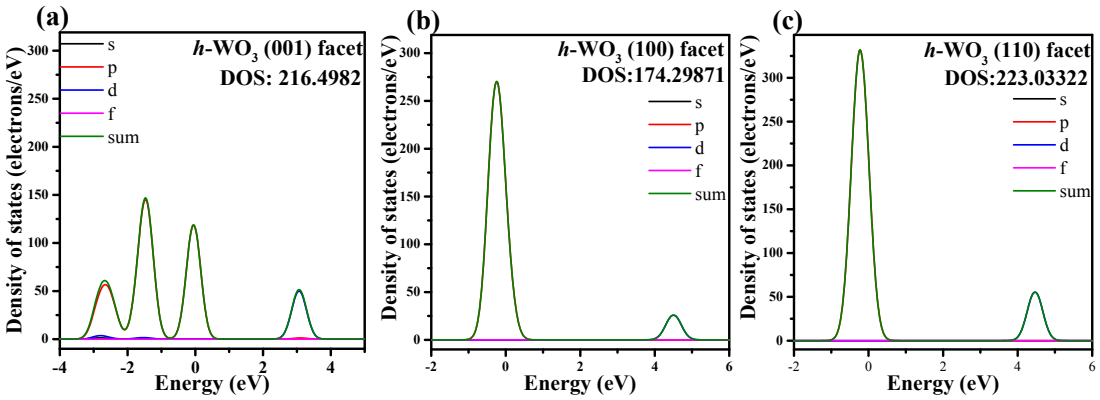

Figure S6 Density of states (DOS) on different crystal planes of Hexagonal WO_3 with different crystal planes. **(**a): WO_3 nanosheets-(001); (b): WO_3 nanoparticles-(110) (c): WO_3 nanobelts-(002); (d): WO_3 nanobelts-(100).

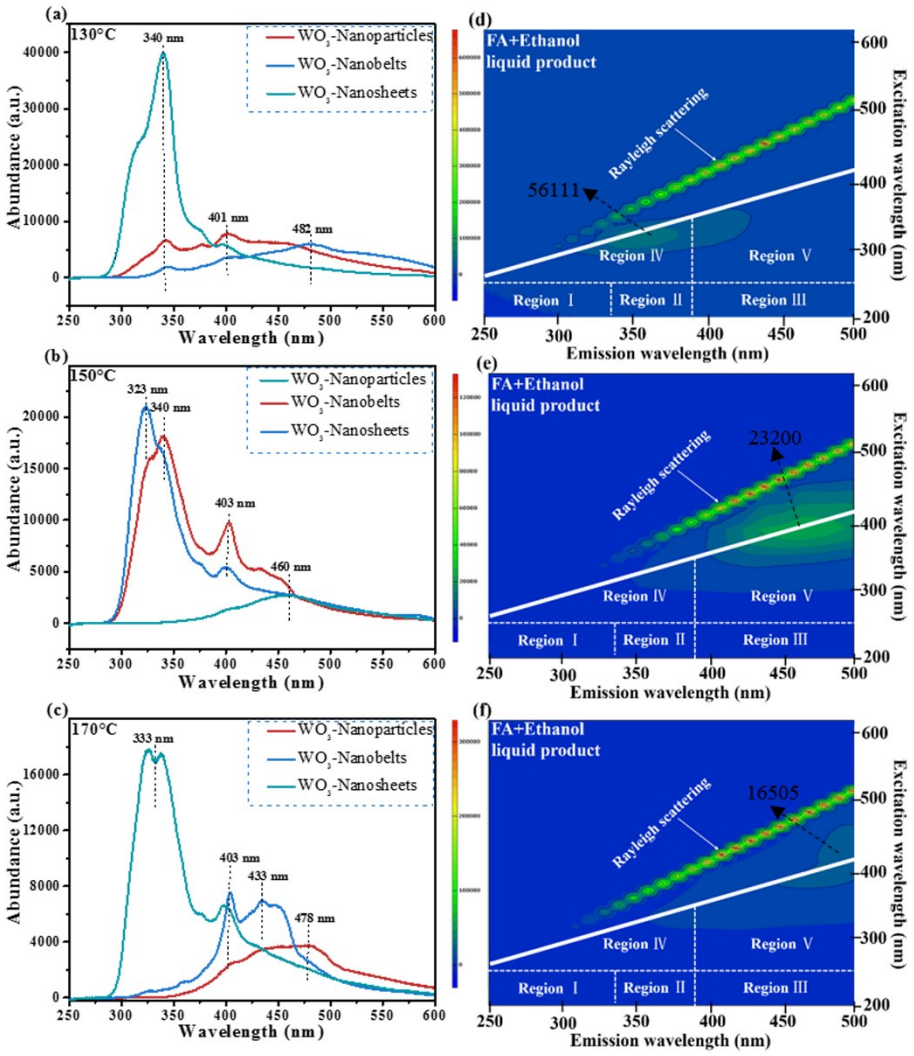

Fig. S7 UV-fluorescence spectra of soluble polymers from the conversion of FA over *h*-WO_3 catalysts. (a) 130ºC, (b) 150ºC, (c) 170ºC, (d) WO_3 nanosheets-150ºC, (e) WO_3 nanobelts-150ºC, and (f) WO_3 nanoparticles-150ºC. (The concentration of the liquid was 400 ppm. The fluorescence peaks at 300~340 nm were attributed to the compounds with one to three fused benzene rings. The fluorescence peaks at 400~482 nm were attributed to the compounds with three to five fused benzene rings.)

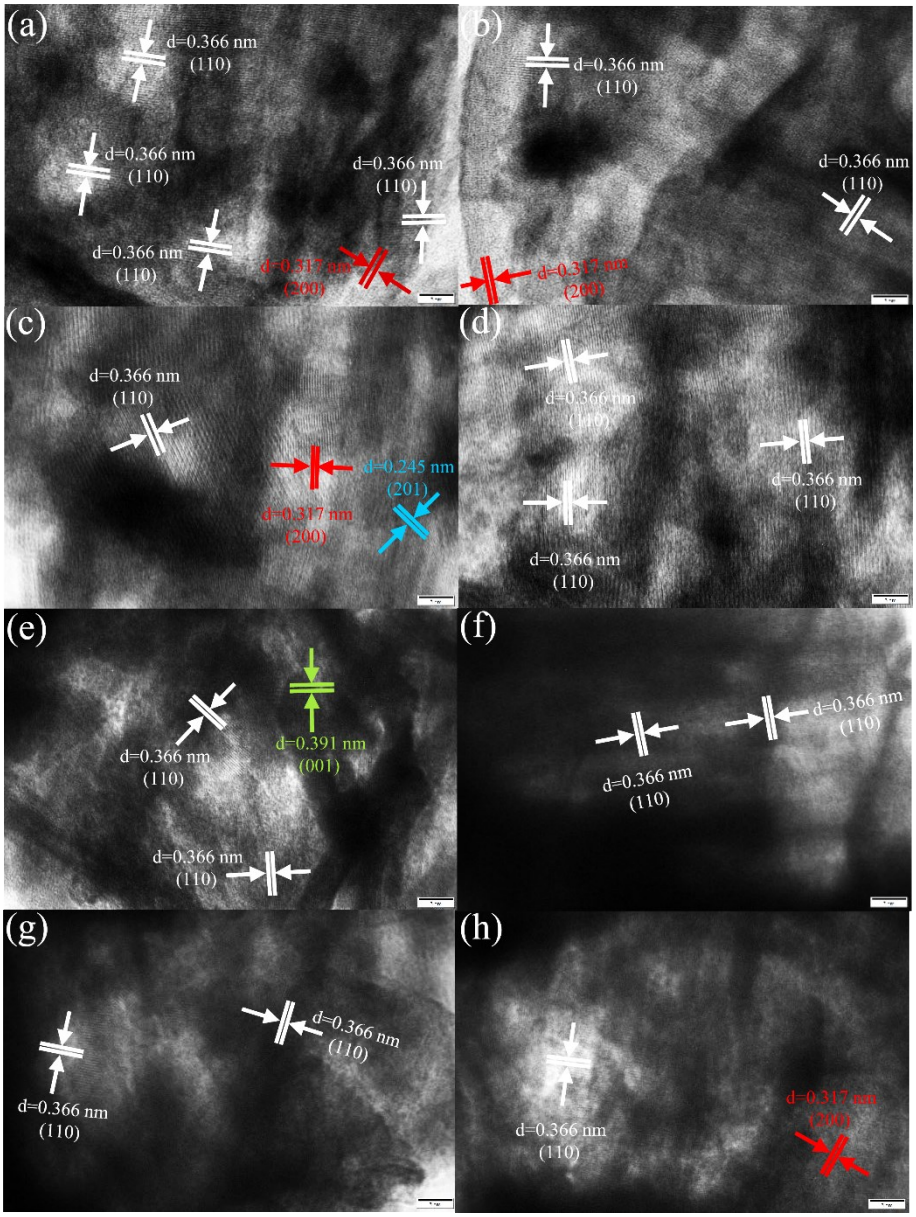

Fig. S8 HRTEM images of WO_3 Nanoparticles.

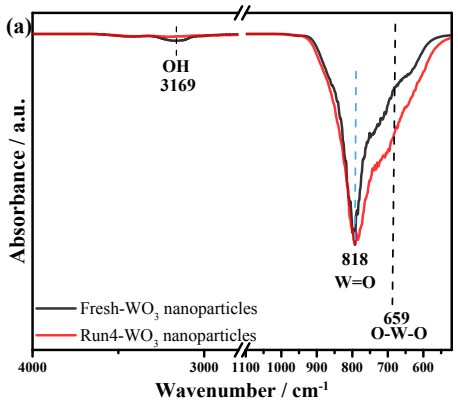

Fig. S9; **(a)** FT-IR spectra of the recovered catalyst and the fresh one.

As shown in Fig. S8, the peaks at 818 and 659 $cm^{-1}$are assigned to the W=O and the O–W–O bond, respectively,which are the typical functional group of WO_3. After four cycles, the strong vibration peaks of the W=O and O–W–O bond demonstrate that the WO_3 nanopartciles has the good stability. However, the peak of –OH at 3169 cm^{-1} shows that Brønsted acid sites are reduced.